

# Punching performance of RC slab-column connections with inner steel truss

Qingxuan Shi<sup>1,2</sup>, Ge Ma<sup>\*1</sup>, Jiangran Guo<sup>1,3</sup> and Chenchen Ma<sup>2,3</sup>

<sup>1</sup> School of Civil Engineering, Xi'an University of Architecture and Technology, Xi'an, Shaanxi, P.R. China

<sup>2</sup> State Key Laboratory of Green Building in Western China, Xi'an, Shaanxi, P.R. China

<sup>3</sup> Key Lab of Structural Engineering and Earthquake Resistance of the Ministry of Education, Xi'an University of Architecture and Technology, Xi'an, Shaanxi, P.R. China

(Received April 12, 2020, Revised July 5, 2022, Accepted October 8, 2022)

**Abstract.** As a brittle failure mode, punching-shear failure can be widely found in traditional RC slab-column connections, which may lead to the entire collapse of a flat plate structure. In this paper, a novel RC slab-column connection with inner steel truss was proposed to enhance the punching strength. In the proposed connection, steel trusses, each of which was composed of four steel angles and a series of steel strips, were pre-assembled at the periphery of the column capital and behaved as transverse reinforcements. With the aim of exploring the punching behavior of this novel RC slab-column connection, a static punching test was conducted on two full-scaled RC slab specimens, and the crack patterns, failure modes, load-deflection and load-strain responses were thoroughly analyzed to explore the contribution of the applied inner steel trusses to the overall punching behavior. The test results indicated that all the test specimens suffered the typical punching-shear failure, and the higher punching strength and initial stiffness could be found in the specimen with inner steel trusses. The numerical models of tested specimens were analyzed in ABAQUS. These models were verified by comparing the results of the tests with the results of the analyzes, and subsequently the sensitivity of the punching capacity to different parameters was studied. Based on the test results, a modified critical shear crack theory, which could take the contribution of the steel trusses into account, was put forward to predict the punching strength of this novel RC slab-column connection, and the calculated results agreed well with the test results.

**Keywords:** critical shear crack theory; punching behavior; punching strength; RC slab-column connection; steel truss

## 1. Introduction

Although RC flat plate structures are widely applied in residential buildings for the purposes of low story height and fast construction, the punching-shear failure, which occurs in the slab-column connections, is still a safety concern in current RC flat plate structures (Kee *et al.* 2019, Tovi *et al.* 2017). As reported in past earthquakes, brittle punching-shear failures could be frequently found in the slab-column connections, which may lead to the entire collapse of a flat plate structure. Therefore, it should be the priority in the structural design of RC flat plate structures to ensure the safety and reliability of the slab-column connections.

As an alternative solution, the shear or punching-shear strength of RC members can be improved by inducing additional steel reinforcements (Abu-Obeidah *et al.* 2019). The research investigates the effect of externally bonded CFRP sheets on the load-carrying capacity of shear-deficient RC beams when attached to the beam's soffit (Hawileh *et al.* 2015). In order to enhance the punching strength of RC slab-column connections, many types of transverse reinforcement were proposed by researchers, and

the representatives are stirrups, shear studs and bar trusses (Adetifa and Polak 2005, Park *et al.* 2007, Eder *et al.* 2010, Hegger *et al.* 2010, Lips *et al.* 2012, Dam and Wight 2016, Einpaul *et al.* 2016, Dam *et al.* 2017, Eom *et al.* 2017, 2018, Kang *et al.* 2017, Broms 2019). As a traditional transverse reinforcement, stirrups are inconvenient to apply in the thin floor slab, and the construction of some other additional transverse reinforcements, whose contribution is similar to stirrups, is quite difficult because the anchorage engages the slab bars. Currently, shear studs and bar truss are popular because they all can be prefabricated in factory and are convenient to assemble on construction sites. Although the punching strength and deformability can be significantly improved by employing the bar truss, the application of steel truss, which is composed of steel angles and a series of steel strips, in the traditional RC slab-column connections is superior in the convenient welding procedure and the diversification of steel section shapes. Meanwhile, the larger superficial area of the upper chords, namely, the steel angles, can collaborate more adjacent concrete to form a composite truss, which may further improve the punching behavior.

In this paper, a novel RC slab-column connection with inner steel truss was proposed to achieve better structural and constructional performances. As shown in Fig. 1, in the proposed connection, steel trusses, each of which was composed of four steel angles and a series of steel strips, were pre-assembled at the periphery of the column capital

\*Corresponding author, Ph.D. Candidate,  
E-mail: mage@live.xauat.edu.cn

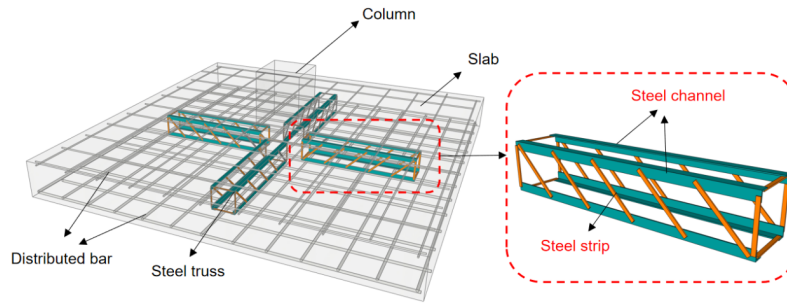


Fig. 1 Diagram of inner steel truss

Table 1 Specimen design

ID	Slab dimensions	Rebar in slab		Column dimensions	Rebar in column			Steel truss	
		Top	Bottom		Bar	Stirrup	Chord	Web	
ST00	2350 mm × 2350 mm	C8@100	C14@90	300 mm × 300 mm	8C18	C8@50	-	-	-
ST01	× 240 mm	C8@100	C14@90	× 400 mm	8C18	C8@50	L20 × 3 mm	10 mm × 188 mm × 3 mm	

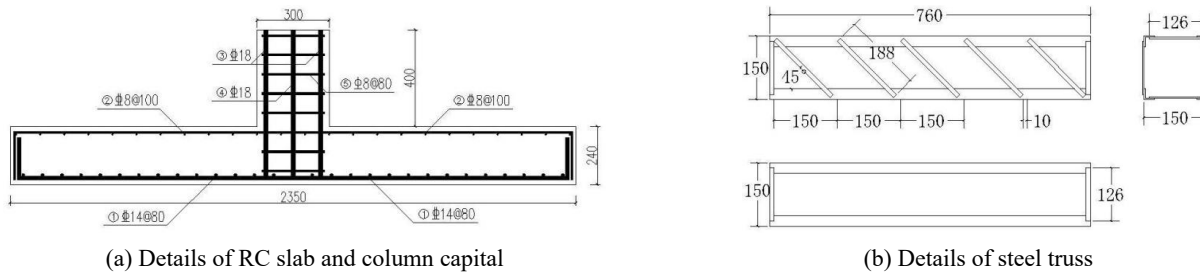


Fig. 2 Specimen design

and behaved as transverse reinforcements. In view of constructability, the steel truss can be prefabricated by welding in factory, and the regular and smooth surface of the steel components can lead to a better welding quality and a higher anchorage strength compared with the bar truss. Meanwhile, the pre-assembled steel trusses can be located between the top and bottom slab bars without engaging these bars, indicating that the placement of these steel trusses is convenient. With the aim of exploring the punching behavior of this novel RC slab-column connection, a static punching test was conducted on two large-scaled RC slab specimens, and the crack patterns, failure modes, load-deflection and load-strain responses were thoroughly analyzed to explore the contribution of the applied inner steel trusses to the overall punching behavior. Based on the test results, a modified critical shear crack theory, which could take the contribution of the steel truss into account, was put forward to predict the punching strength of this novel RC slab-column connection later in this paper.

## 2. Experimental program

### 2.1 Specimen design

Two large-scaled slab-column connections were designed and tested, and the geometry and flexural

reinforcements were identical of these two specimens. The first specimen was fabricated without inner steel truss, labeled as ST00, which could be regarded as a control specimen. As shown in Fig. 1, the other specimen, labeled as ST01, was reinforced using four inner steel trusses, whose layout was cruciform.

As shown in Fig. 2(a), the overall dimensions of the RC slabs were 2350 mm × 2350 mm × 240 mm, and those of the column capitals were 300 mm × 300 mm × 400 mm. The thicknesses of the concrete cover in the slab and column capital were 20 mm and 25 mm, respectively. For the flexural reinforcements which were located at the top surface of RC slab, C8 bars, indicating that the diameter of the rebar was 8 mm and the strength grade was HRB 400 as per Chinese codes, were distributed both along the  $x$  and  $y$  directions at a spacing of 100 mm (reinforcement ratio  $\rho_c = 0.002$ ). For the flexural reinforcements which were located at the bottom surface of RC slab, C14 bars were distributed both along the  $x$  and  $y$  directions at a spacing of 90 mm (reinforcement ratio  $\rho_t = 0.007$ ). Meanwhile, the column capitals were longitudinally reinforced using 8C18 bars and transversely confined using C8 bars at a spacing of 80 mm. As shown in Fig. 2(b), the steel truss was composed of four steel angles and a series of steel strips, and the inclination between the steel angle and the diagonal steel strips was 45°. The strength grades of the applied steel angles and strips were both Q235, and the applied steel angles were

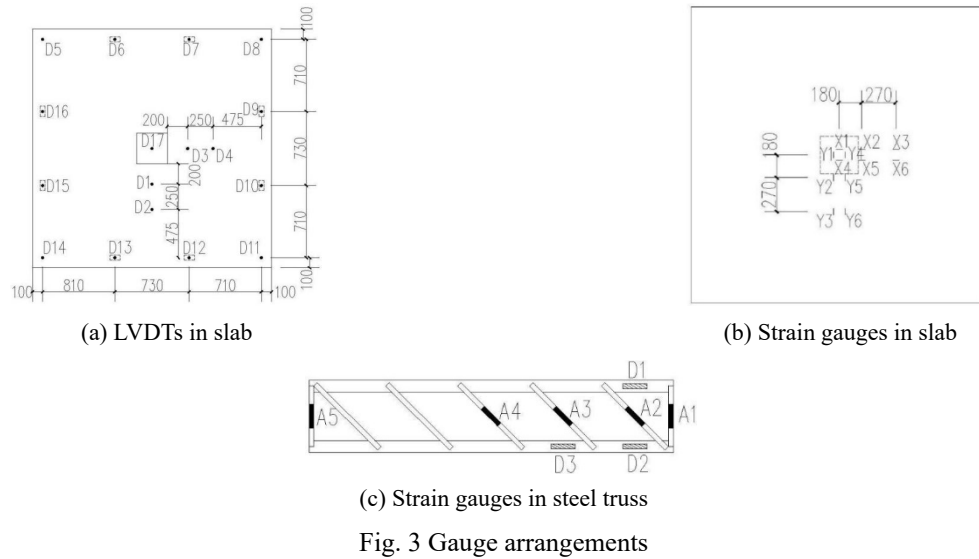


Fig. 3 Gauge arrangements

L20 per Chinese codes, indicating that the length of the steel rib was 20 mm. Meanwhile, the thicknesses of the applied steel angles and steel strips were both 3 mm.

The construction of the test specimens could be divided into three steps. In the first step, the bottom rebar grid of the RC slab and the steel skeleton of the column capital were assembled. In the second step, as shown in Fig. 1, a total of four prefabricated steel trusses were connected to the steel skeleton of the column capital using spot welding, and the layout was cruciform. Finally, the top rebar grid of the RC slab was assembled and the specimens were cast using normal weight concrete.

## 2.2 Material properties

All the specimens were cast using normal-weight and ready-mixed concrete. Several concrete cubes with the dimensions of 150 mm × 150 mm × 150 mm were prepared with the same period as the specimens casting, and the average tested compressive strength of these concrete cubes was 42.83 MPa. For the mechanical properties of rebar reinforcements, the yield strengths of the top/bottom slab bars and column bars, C8, C14 and C18, were 464.47 MPa, 430.21 MPa and 440.00 MPa, respectively. For the mechanical properties of the steel trusses, the yield strengths of the steel angles and steel strips were 313.93 MPa and 324.97 MPa, respectively. The detailed properties of applied steel reinforcements are recorded in Table 2.

## 2.3 Loading device and gauge arrangements

The loading device is illustrated in Fig. 4. As shown in Fig. 4, the specimens were simply supported by four rollers along the perimeter of the slab with the aim of a feasible testing condition in the structural lab, and four thick steel plates were placed on the four steel rollers to avoid the local crushing of the concrete near the roller supports.

A hydraulic jack with a maximum capacity of 5000 kN and a maximum stroke of 200 mm was employed to apply the vertical downward force on the column capital. In order to spread the vertical force over the entire column section

Table 2 Mechanical properties of steel reinforcements

Material	Type	Yield strength $f_y$ /MPa	Ultimate strength $f_u$ /MPa
Rebar	Φ 8	464.47	659.13
	Φ 14	430.21	629.92
	Φ 18	440.00	640.00
Steel truss	Angle	313.93	444.11
	Strip	324.97	447.14

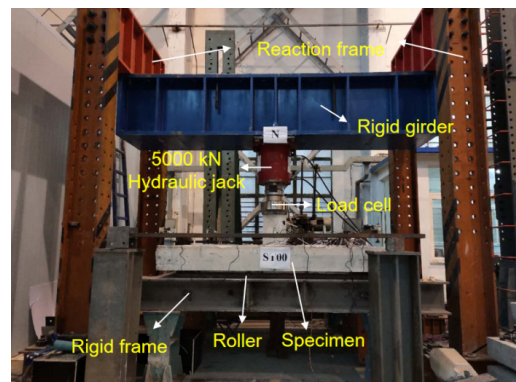


Fig. 4 Loading device

uniformly, a steel pad was placed on the column capital, and the applied vertical force was monitored using a load cell which was located between the jack and the steel pad.

For the loading procedure, the punching test was performed by increasing the slab deflection (jack stroke) gradually, and the vertical load was held constant to record the development of cracks in the slab. When the maximum load recorded, the specimens were pushed downward continuously until the punching cone of concrete was obviously formed.

The detailed gauge arrangements are thoroughly illustrated in Fig. 3. As shown in Fig. 3(a), a total of 17 Linear Variable Differential Transformers (LVDTs) were

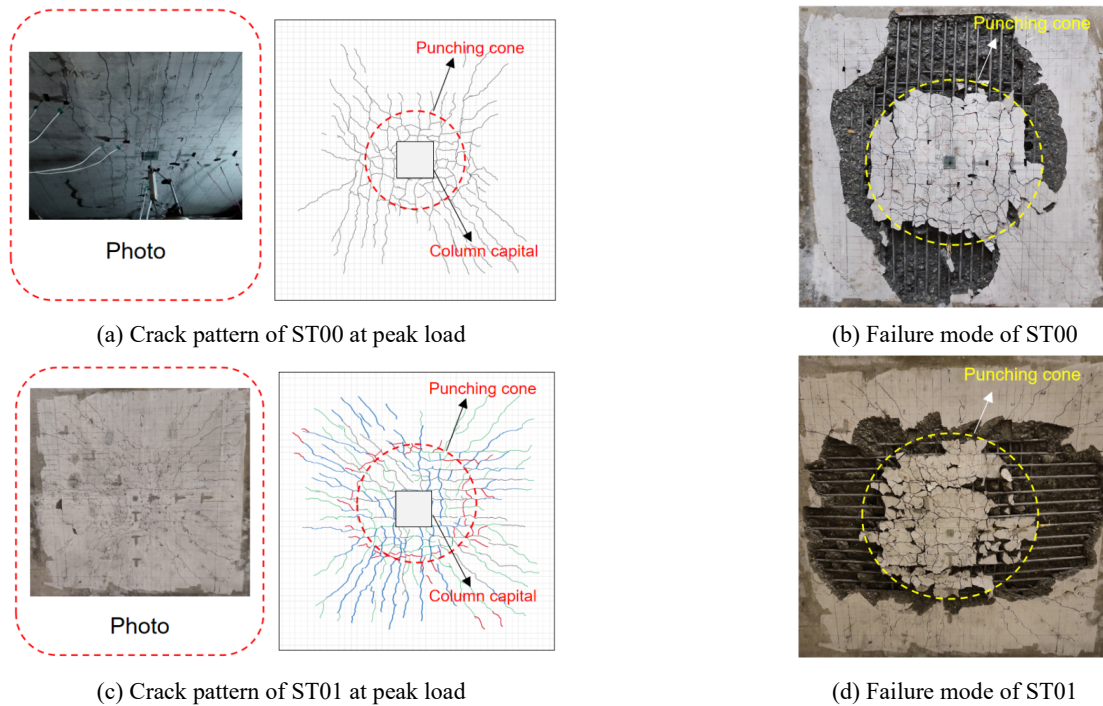


Fig. 5 Crack patterns and failure modes

applied to record the deflection developments at the supports, loading point and shear spans. As shown in Figs. 3(b)-(c), strains of flexural bars and steel trusses were monitored using electronic strain gauges to further analyse the failure modes.

### 3. Experimental results

#### 3.1 Crack patterns and failure modes

The crack patterns and failure modes of the test specimens were illustrated in Fig. 5, in which photographs were taken from the bottom surface of the slab. Figs. 5(a) and (c) depict the two-way cracks for the bottom surface of the slab, and it is obvious that numerous two-way cracks could be found along both radial and principal directions when the corresponding maximum load was reached. Meanwhile, more abundant flexural cracks were observed in the specimen reinforced by inner steel trusses, indicating that the existence of steel angles enhance the flexural strength of the slab-column connection. On the other hand, the emergence of these flexural cracks could be regarded as a warning of the final failure.

Generally, the first pack of flexural cracks was captured when the applied vertical load was approximately  $0.5P_u$ , and the radial cracks emerged as the load increased. When the vertical load was approximately  $0.8P_u$ , the gathered radial cracks propagated and formed the bottom surface of the concrete punching cone. After the corresponding maximum load was reached, the specimens were continuously pushed downward, and Figs. 5(b) and (d) show the final failure modes of the test specimens. As shown in these figures, the punching cones could be clearly distinguished, indicating that all the specimens suffered

a typical punching-shear failure. It could be also seen from Figs. 5(b) and (d) that the radius of the punching cone was approximately a distance  $h_0$ , where  $h_0$  is the effective depth of the slab.

#### 3.2 Load-deflection curves

Fig. 6 shows the vertical load-deflection ( $P-\Delta$ ) relationships of the test specimens. In Fig. 6, the horizontal and vertical axes denote the slab deflection  $\Delta$ , which was recorded by the gauge D17 shown in Fig. 4, and the vertical downward load  $P$ , which was measured using the load cell. As shown in Fig. 6, the initial stiffness of ST01 was quite higher than that of ST00, which indicated that the application of the inner steel trusses could increase the stiffness.

Generally, the two specimens behaved in a similar manner without any crack before the column displacement was approximately 7.0 mm, and the load-deflection curves

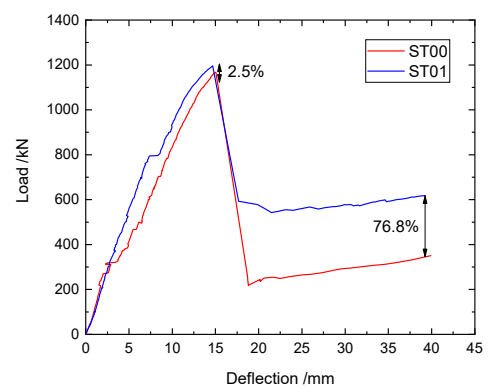


Fig. 6 Load-deflection curves

remained elastic during this period. The first pack of flexural cracks was observed along the column perimeter when the vertical load was approximately 700 kN, and the load-deflection curves of the test specimens both begun to deviate from the elastic response. As the load increased, the specimen ST00 failed at 1167.7 kN, while the specimen ST01 failed at the load of 1195.9 kN. Both the two specimens suffered a significant drop in load after the peak load was reached, which the main reason was the separation of the concrete punching cone around the column perimeter from the slab. After this stage, both the two specimens could hold the corresponding residual load until the punching cone was pushed out.

The peak load of the specimen ST01 was only 2.5% higher than that of the control specimen ST00, and the slight enhancement in peak punching strength could be attributed to the cruciform-arranged steel trusses and the thin web members. After the concrete punching cone around the column perimeter was separated from the slab, the residual strength of the specimen ST00 was mainly provided by the support from the bottom rebar grid. Nevertheless, the inner steel trusses, which connected the slab and the concrete punching cone, could provide more residual strength. Therefore, the residual load of the specimen ST01 was 76.8% higher than that of the specimen ST00.

To conclude, the application of inner steel trusses can both improve the peak punching strength and the post-peak residual strength of the traditional slab-column connections. If a radial layout of steel trusses and thicker steel strips are applied, both the punching strength and the deformability can be further enhanced.

### 3.3 Load-strain curves

Figs. 7(a)-(b) show the strains of the bottom tensile bars of the test specimens. In these figures, X1, X2 and X3 denote the strains monitored from the C 14 bars along the x direction until the corresponding peak load was reached.

As shown in Figs. 7(a)-(b), the bottom tensile bars did not reach the yield strains, indicating that the punching-shear failure occurred before the flexural failure. Fig. 7(c) depicts the strains of the web members of the applied steel trusses, namely, the diagonal steel strips. In these figures, A1, A2, A3 and A4 denote the strains monitored from the

steel strips, and the distances between the column face and the gauges A1, A2 and A4 are increasing. As shown in Fig. 7(c), the strain of the gauge A2, which was mounted on the steel strip whose average distance from the column face was 90 mm, significantly exceeded the yield strain, while the strains of the other gauges did not reach the yield strains. It indicated that the steel strip, where the gauge A2 was located, and the major inclined crack, which caused the punching shear failure, intersected during the loading process and this steel strip could contribute to the punching strength. Meanwhile, it is worth noting that the major inclined crack passed the second web member of the steel truss and the radius of the punching cone was approximately a distance  $h_0$ , indicating that the steel strips located within a distance  $h_0$  from the face of the column capital could contribute the tensile strength to the overall punching strength.

## 4. Finite element model

Finite element analysis is widely regarded as one of the best numerical methods for solving the mathematical problems of engineering. In this research, finite element modeling is performed by the available software ABAQUS.

### 4.1 Concrete damaged plasticity and constitutive laws

The CDP model depicts the inelastic behavior of concrete by combing the concepts of isotropic tensile and compressive plasticity with isotropic damage elasticity. Additionally, this model is generated for predicting the ductile and brittle damages in the regions of compressive and tensile states of stress, respectively, towards the failure state of stress.

The uniaxial compressive behavior of concrete used herein is specified by the stress-strain relationship taken from the modified Hognestad's model as shown. According to this model, the stress-strain relationship can be divided into ascending second-order parabola and descending first-order line. The stress-strain curve of concrete under uniaxial compression is determined by the following formula

$$\sigma = (1 - d_c)E_c\varepsilon \quad (1)$$

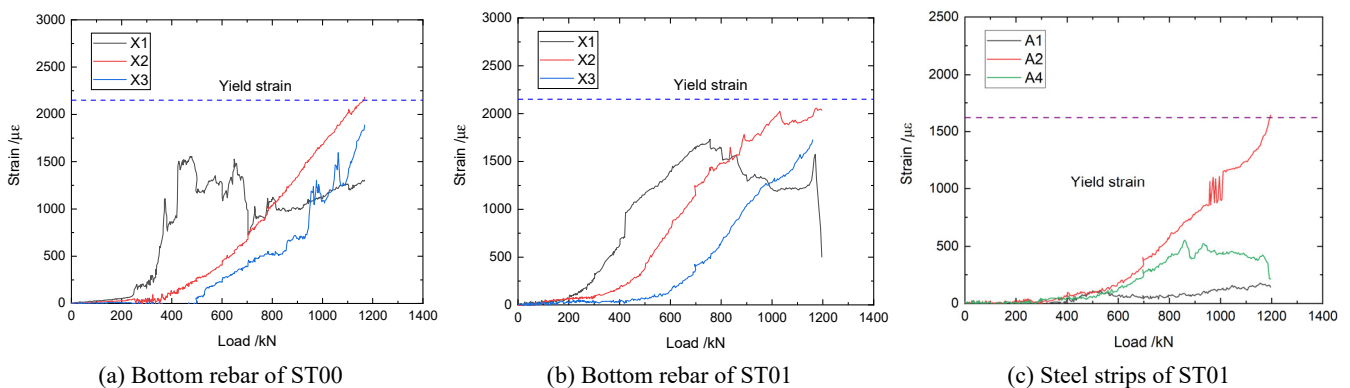


Fig. 7 Load-strain curves

$$d_c = \begin{cases} 1 - \frac{\rho_c n}{n-1+x^n} & x \leq 1 \\ 1 - \frac{\rho_c}{\alpha_c [x-1]^2 + x} & x > 1 \end{cases} \quad (2)$$

$$\rho_c = \frac{f_{c,r}}{E_c \varepsilon_{c,r}} \quad (3)$$

$$n = \frac{E_c \varepsilon_{c,r}}{E_c \varepsilon_{c,r} - f_{c,r}} \quad (4)$$

$$x = \frac{\varepsilon}{\varepsilon_{c,r}} \quad (5)$$

Where,  $\alpha_c$  is the parameter value of the descending section of stress-strain curve of concrete under uniaxial compression;  $f_{c,r}$  represents the uniaxial compressive strength of concrete;  $\varepsilon_{c,r}$  is the peak strain of concrete corresponding to uniaxial compressive strength,  $f_{c,r}$ ;  $d_c$  is the damage evolution parameter of concrete under uniaxial compression. Where

$$\varepsilon_{c,r} = (700 + 172\sqrt{f_{c,r}}) \times 10^{-6} \quad (6)$$

$$\alpha_c = 0.157f_{c,r}^{0.785} - 0.905 \quad (7)$$

The stress-strain curve of concrete under uniaxial tension is determined by the following formula

$$\sigma = (1 - d_t)E_c \varepsilon \quad (8)$$

$$d_t = \begin{cases} 1 - \rho_t(1.2 - 0.2x^5) & x \leq 1 \\ 1 - \frac{\rho_t}{\alpha_t(x-1)^{1.7} + x} & x > 1 \end{cases} \quad (9)$$

$$x = \frac{\varepsilon}{\varepsilon_{t,r}} \quad (10)$$

$$\rho_t = \frac{f_{t,r}}{E_c \varepsilon_{t,r}} \quad (11)$$

Where,  $\alpha_t$  is the parameter value of the descending section of concrete uniaxial tensile stress-strain curve;  $f_{t,r}$  represents the uniaxial tensile strength of concrete;  $\varepsilon_{t,r}$  is the peak strain of concrete corresponding to uniaxial tensile strength,  $f_{t,r}$ ;  $d_t$  is the uniaxial tensile damage evolution parameter of concrete. Where

$$\varepsilon_{t,r} = f_{t,r}^{0.54} \times 65 \times 10^{-6} \quad (12)$$

$$\alpha_t = 0.312f_{t,r}^2 \quad (13)$$

Lemaitre's strain equivalence principle was used to transform the damage evolution parameters into damage factors in the CDP model.

$$D_c = 1 - \sqrt{1 - d_c} \quad (14)$$

$$D_t = 1 - \sqrt{1 - d_t} \quad (15)$$

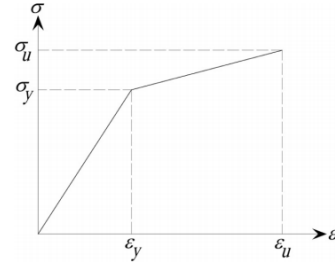


Fig. 8 Stress-strain relationship for steel reinforcement

$D_c$ ,  $D_t$  are compression damage factor and tension damage factor respectively.

In ABAQUS software concrete compressive and tensile stress and strain calculation parameters according to the type, CDP model also needs some other parameters, including the expansion Angle  $\psi = 30^\circ$ , eccentricity  $\delta = 0.1$ , biaxial compressive strength and uniaxial compressive ultimate strength ratio  $f_{b0}/f_{c0} = 0.5$ , the second stress constant tensile radial compression meridian  $K_c = 2/3$  and viscous parameters of  $u = 0.005$ .

#### 4.2 Steel reinforcement properties

Steel reinforcement behaves the same as the elastic plastic material associated with the strain hardening, as shown in Fig. 8. The steel material properties are specified by the value of yield and ultimate strains,  $\varepsilon_y$  and  $\varepsilon_u$ , yield and ultimate stresses,  $\sigma_y$  and  $\sigma_u$ , and modulus of elasticity,  $E_s$ . In this study, the load transfer mechanism from steel reinforcement to concrete and vice versa was based on the assumption that the perfect bond between the reinforcing bars and its surrounding concrete exists. To prevent numerical instability in the plastic phase, a small positive value was added to the slope of the strain stress diagram in the plastic criteria.

#### 4.3 Element specifications

C3D8R element was used for the ordinary concrete, and T3D2 element was used for reinforcing bars and truss bars. Therefore, slip behavior between concrete slab and truss bars was defined as embedded. Mesh size of elements in concrete and reinforcing bars was 30 mm, and mesh size of truss bars was 10 mm.

#### 4.4 Boundary conditions

All of the RC slabs were simply supported along the four edges. The concentrated load was monotonically subjected to the center point of the slabs, where a stiff steel plate was centrally placed on them. To model the loading scheme, the vertical displacement corresponding to the maximum load was applied to the slabs, more precisely, the displacement control method was implemented to investigate the behavior of the slabs.

#### 4.5 Properties of the RC slabs models

The two experimental specimens were modeled as M00

Table 3 Model design detail

Model name	Distance	Angle
M00	—	—
M01	150	45°
D120	120	45°
D90	90	45°
D60	60	45°
A60	120	60°
A30	120	30°

and M01. Another 5 numerical models were built base on M01 which have differences in steel truss design. The distances and angle of the steel strips were considered as sensitivity parameters. The distances of the steel strips in trusses are 150 mm, 120 mm, 90 mm and 60 mm in model M01, D120, D90 and D60 respectively. The angle of steel strips between the steel channel is 45°, 60°, 30° in trusses of model M01, A60, A30 respectively.

The model design was shown in Table 3.

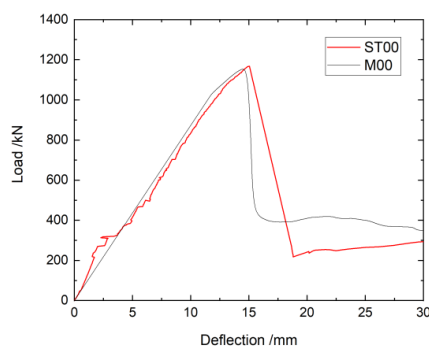
## 5. Comparison of the results

### 5.1 Compared with the test result

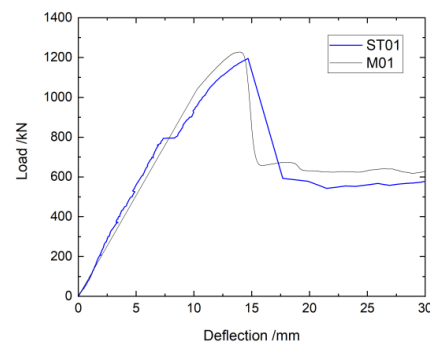
Fig. 9 shows the calculated load-deflection curves of M00 and M01 compared with the test curves of specimens ST00 and ST01. The results show that the finite element model established in this chapter can better simulate the load-deflection curves of the punching failure of RC plate column joints, and the ratio of the test value and simulation value of peak load is 0.987 and 1.026, the corresponding ratio of plate center deflection is 0.963 and 0.952. Good results are obtained in the failure load and the corresponding plate center deflection. Therefore, it can be considered that the parameter settings in the finite element model are reasonable, which can accurately simulate the whole process of punching shear behavior of RC plate column joints.

### 5.2 Influence of the steel strip distance

Fig. 10 shows the influence of spacing between belly



(a) ST00&amp;M00



(b) ST01&amp;M01

Fig. 9 Load-deflection curves

bars on punching capacity of reinforced concrete slab column joints. The punching capacity of plate column joints increases with the increase of the number of belly bars. When the distance between the belly bars is small, it will restrain both sides of the surrounding oblique concrete bars. However, when the spacing is too large, the spatial function of the truss is basically invalid and cannot play a role together.

Based on M01, the punching capacity of plate column joints of model D120, D90 and D60 increased by 0.73%, 2.08% and 4.72% respectively. When the spacing of the ventral rod is reduced to a certain extent, the punching bearing capacity of the plate column joint will not increase proportionally with the decrease of the spacing of the ventral rod. Combined with the steel content of the plate column joint, it is not suitable to set too many ventral rods.

### 5.3 Influence of the steel strip angle

Fig. 11 shows the influence of the angle between the belly and chord of steel truss on the punching capacity and ductility of reinforced concrete slab column joints. Based on model M01, the punching capacity of plate column joints of model A60 and A30 increased by 0.53% and -2.69% respectively. The research shows that the horizontal angle between the punching failure cone and the plate surface of the plate column joint is not 45° as shown in the Chinese code. According to a large number of test results, the angle of punching failure cone is 26°-30°. Therefore, the closer the angle formed between the belly rod and the punching

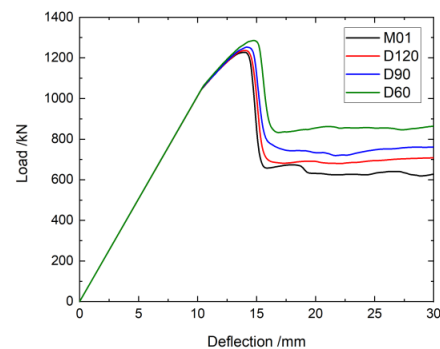


Fig. 10 Load-deflection curves of Models with different strip distance

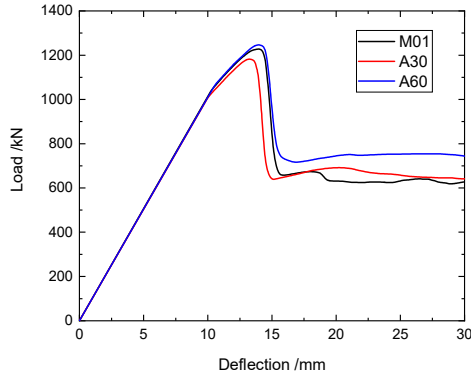


Fig. 11 Load-deflection curves of Models with different strip angle

failure cone is to 90, the stronger the punching resistance of the belly rod will be.

## 6. Prediction of punching strength

In order to comprehensively reflect the impact of steel strip size, spacing and strip angle on the punching performance of slab-column joints with internal steel truss. The concept of steel ratio of truss strip  $\rho_v$  is put forward in this paper.

$$\rho_v = \frac{A_s}{u_m \cdot \max(s_0 + s_1/2; s_1)} \quad (16)$$

$A_s$  is the area of all steel strip sections intersecting within the critical section perimeter;  $U_m$  is the critical section perimeter, and the section perimeter is taken at the effective plate height 0.5 from the column edge.  $S_0$  is the distance from the center point of the nearest strip to the edge of the column;  $S_1$  is the spacing between steel strips.

As for the specimens and models mentioned before, the

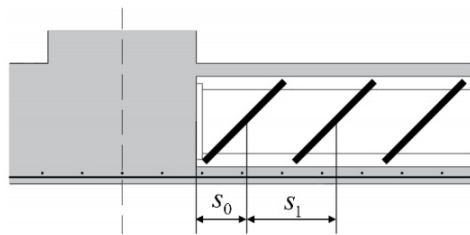


Fig. 12 Parameter of steel ratio

Table 4 The steel ratio of truss strips

Specimens	$A_s/\text{mm}^2$	$S_0/\text{mm}$	$S_1/\text{mm}$	$\rho_v$
ST01/M01	240	90	150	0.0699%
D120	240	90	120	0.0769%
D90	360	90	90	0.1282%
D60	360	90	60	0.1442%
A60	240	42	150	0.0769%
A30	240	125	150	0.0577%

steel ratios of truss strips were shown in Table 4.

The critical shear crack theory was applied and modified with the steel ratio  $\rho_v$  here to predict the punching strength of the test specimens (Muttoni 2008, Ruiz and Muttoni 2009). The critical shear crack theory was proposed by Muttoni and was capable to calculate the punching strength of traditional RC slab-column connections precisely. Based on the rotation of a RC slab, the critical shear crack theory proposed a failure law for punching behavior, and the punching strength can be obtained by calculating the intersection of the failure criterion and the load-rotation relationship from a simple mechanical model, as shown in Fig. 8(a).

The load-rotation relationship can be determined using the following equations

$$\psi = 0.33 \frac{L f_y}{d E_s} \left( \frac{V_d}{8m_R} \right) \quad (17)$$

$$m_R = \rho f_y d^2 \left( 1 - \frac{\rho f_y}{2f_c} \right) \quad (18)$$

where  $\psi$  is the rotation of a RC slab;  $L$  is the main span of a RC slab;  $d$  is the distance from extreme compression fiber to the centroid of the longitudinal tensile rebar of a RC slab;  $f_y$  is the yield strength of the longitudinal tensile rebar;  $E_s$  is the modulus of elasticity of the steel reinforcements;  $V_d$  is the vertical load;  $m_R$  is the moment capacity per unit width;  $\rho$  is the reinforcement ratio of the longitudinal tensile rebar;  $f_c$  is the compressive strength of concrete.

The failure criterion can be obtained using the following equations

$$V_R = V_c + k_v \rho_v V_s \quad (19)$$

$$V_c = \frac{3}{4} \frac{b \sqrt{f_{c0, int}}}{1 + 15 \frac{\psi d}{d_{g0} + d_g}} \quad (20)$$

$$V_s = \frac{E_s \psi}{6} A_{sw} \sin \theta \leq f_{ys} A_{sw} \quad (21)$$

where  $V_R$  is the punching strength;  $V_c$  is the contribution of the reinforced concrete;  $V_s$  is the contribution of the inner steel truss;  $b_0, int$  is the control perimeter, which can be defined at  $d/2$  beyond the crack tip, typically at the column face;  $d_{g0}$  is a reference aggregate size,  $d_{g0} = 16$  mm;  $d_g$  is the maximum aggregate size of the applied concrete;  $A_{sw}$  is the total cross-sectional area of steel strips within a perimeter at  $d$  from the column face;  $\theta$  is the inclination between the steel strip and the steel angle.  $\rho_v$  is the steel ratio of truss strips which is defined in Eq. (16). And  $k_v$  is the correction factor of  $\rho_v$ , taken  $k_v = 700$  from experience (Jiang 2020).

The predicted load-rotation relationship and the failure criterion of the test specimens can be obtained by substituting the design parameters into Eqs. (17)-(21), and the calculate results are shown in Table 5. As shown in Fig. 13, the calculated punching strengths of the specimens ST00 and ST01 are 1163.44 kN and 1193.36 kN, respectively. Meanwhile, the ratios of calculated to tested

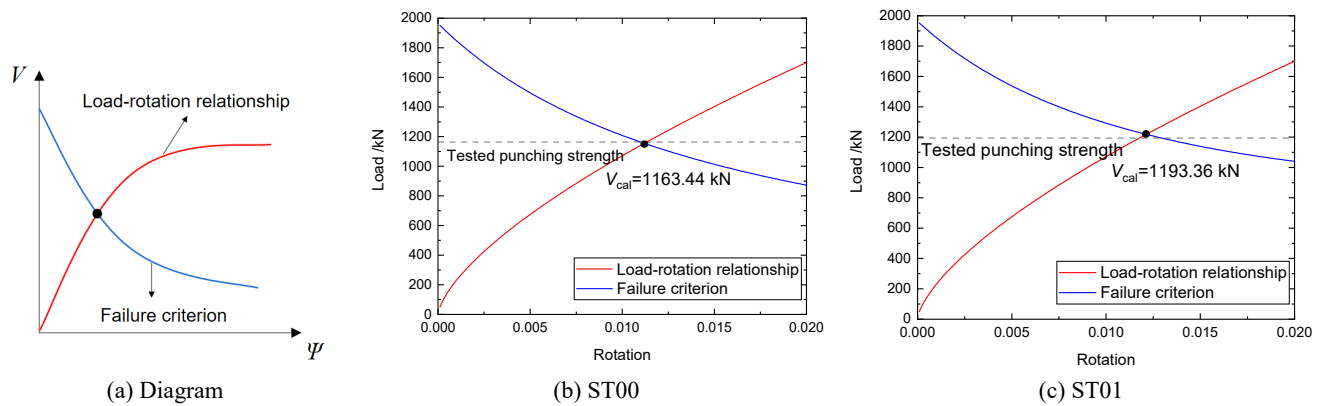


Fig. 13 Punching strength prediction using the modified critical shear crack theory

Table 5 Comparison of the predicted strength

Specimen	$V_U/kN$	$\rho_v$	$V_{cal}/kN$	$V_{cal}/V_U$
ST00	1167.7	0	1163.44	0.996
ST01	1195.9	0.0699%	1193.36	0.998
D120	1236.56	0.0769%	1196.49	0.968
D90	1253.03	0.1282%	1252.55	1.001
D60	1285.75	0.1442%	1293.27	1.006
A60	11234.05	0.0769%	1229.32	0.996
A30	1182.18	0.0577%	1187.94	1.005

punching strengths of the specimens ST00 and ST01 are 0.996 and 0.998, respectively. Compared with the finite element model result, the ratios range from 0.968 to 1.006. It indicates that the modified critical shear crack theory can calculate the punching strength of this novel RC slab-column connection with inner steel truss rationally.

## 7. Conclusions

Through the punching shear tests of a novel RC slab-column connection with inner steel truss and a traditional RC slab-column connection, the crack patterns, failure mode and shear-resisting mechanism were investigated. The primary conclusions and findings of this paper can be listed as follows:

- (1) During the failure period, the concrete punching cones could be clearly distinguished in all the test specimens, indicating that both the novel RC slab-column connection with inner steel truss and the traditional RC slab-column connection suffered a typical punching-shear failure. More abundant flexural cracks could be observed in the specimen reinforced by inner steel trusses, which could be regarded as a warning of the final failure.
- (2) The application of inner steel trusses could both improve the peak punching strength and the post-peak residual strength of the traditional slab-column connections. If a radial layout of steel trusses and thicker steel strips are applied, both the punching strength and the deformability can be further

The application of inner steel trusses could both improve the peak punching strength and the post-peak residual strength of the traditional slab-column connections. If a radial layout of steel trusses and thicker steel strips are applied, both the punching strength and the deformability can be further enhanced.

- (3) The numerical models of tested specimens were analyzed in ABAQUS. These models were verified by comparing the results of the tests with the results of the analyses, and subsequently the sensitivity of the punching capacity to different parameters was studied. As the results shown, the optimum angle of truss strip is perpendicular to the punching failure cone, while the angle of punching failure cone is  $26^\circ$ - $30^\circ$  usually. The punching capacity of plate column joints increases with the increase of the number of belly bars. When the distance between the belly bars is small, it will restrain both sides of the surrounding oblique concrete bars.
- (4) Based on the test and numerical models results, a modified critical shear crack theory, which could take the contribution of the steel truss into account, was put forward to predict the punching strength of this novel RC slab-column connection, and the calculated results agreed well with the test results.

## Acknowledgments

The experiment mentioned in this paper was funded by the National Natural Science Foundation of China (Grant No. 51878540). The financial support is highly appreciated.

## References

- Abu-Obeidah, A.S., Abdalla, J.A. and Hawileh, R.A. (2019), "Shear strengthening of deficient concrete beams with marine grade aluminium alloy plates", *Adv. Concrete Constr., Int. J.*, 7(4), 249-262. <https://doi.org/10.12989/acc.2019.7.4.249>
- Adetifa, B. and Polak, M.A. (2005), "Retrofit of slab column interior connections using shear bolts", *ACI Struct. J.*, 102(2), 268-273.
- Broms, C.E. (2019), "Cages of Inclined Stirrups as Shear Reinforcement for Ductility of Flat Slabs", *ACI Struct. J.*

- 116(1), 83-92. <http://dx.doi.org/10.14359/51710871>
- Dam, T.X. and Wight, J.K. (2016), "Flexurally-triggered punching shear failure of reinforced concrete slab-column connections reinforced with headed shear studs arranged in orthogonal and radial layouts", *Eng. Struct.*, **110**, 258-268. <http://dx.doi.org/10.1016/j.engstruct.2015.11.050>
- Dam, T.X., Wight, J.K. and Parra-Montesinos, G.J. (2017), "Behavior of Monotonically Loaded Slab-Column Connections Reinforced with Shear Studs", *ACI Struct. J.*, **114**(1), 221-232.
- Eder, M.A., Vollum, R.L., Elghazouli, A.Y. and Abdel-Fattah, T. (2010), "Modelling and experimental assessment of punching shear in flat slabs with shearheads", *Eng. Struct.*, **32**(12), 3911-3924. <http://dx.doi.org/10.1016/j.engstruct.2010.09.004>
- Einpaul, J., Brantschen, F., Ruiz, M.F. and Muttoni, A. (2016), "Performance of punching shear reinforcement under gravity loading: influence of type and detailing", *ACI Struct. J.*, **113**(4), 827-838. <http://dx.doi.org/10.14359/51688630>
- Eom, T.S., Song, J.W., Song, J.K., Kang, G.S., Yoon, J.K. and Kang S.M. (2017), "Punching-shear behavior of slabs with bar truss shear reinforcement on rectangular columns", *Eng. Struct.*, **134**, 390-399. <http://dx.doi.org/10.1016/j.engstruct.2016.12.048>
- Eom, T.S., Kang, S.M., Choi, T.W. and Park, H.G. (2018), "Punching Shear Tests of Slabs with High-Strength Continuous Hoop Reinforcement", *ACI Struct. J.*, **115**(5), 1295-1305. <http://dx.doi.org/10.14359/51702231>
- Hawileh, R.A., Nawaz, W., Abdalla, J.A. and Saqan, E.I. (2015), "Effect of flexural CFRP sheets on shear resistance of reinforced concrete beams", *Compos. Struct.*, **122**, 468-476. <http://dx.doi.org/10.1016/j.compstruct.2014.12.010>
- Hegger, J., Ricker, M. and Sherif, A.G. (2010), "Punching Strength of Reinforced Concrete Footings", *ACI Struct. J.*, **107**(4), 494-496.
- Jiang, M.Y. (2020), "Research on punching shear capacity of concrete slab-column connections with steel truss", M.Sc. Dissertation; Xi'an University of Architecture and Technology, Xi'an, China.
- Kang, T.H.K., Lee, J.D., Lee, B.S., Kim, M.J. and Kim, K.H. (2017), "Punching and Lateral Cyclic Behavior of Slab-Column Connections with Shear Bands", *ACI Struct. J.*, **114**(5), 1075-1086. <http://dx.doi.org/10.14359/51689780>
- Kee, J.H., Park, H.Y. and Seong, J.H. (2019), "Effect of one way reinforced concrete slab characteristics on structural response under blast loading", *Adv. Concrete Constr., Int. J.*, **8**(4), 277-283. <https://doi.org/10.12989/acc.2019.8.4.277>
- Lips, S., Ruiz, M.F. and Muttoni, A. (2012), "Experimental investigation on punching strength and deformation capacity of shear-reinforced slabs", *ACI Struct. J.*, **109**(6), 889-900.
- Muttoni, A. (2008), "Punching shear strength of reinforced concrete slabs without transverse reinforcement", *ACI Struct. J.*, **105**(4), 440-450.
- Park, H.G., Ahn, K.S., Choi, K.K. and Chung, L. (2007), "Lattice shear reinforcement for slab-column connections", *ACI Struct. J.*, **104**(3), 294-303.
- Ruiz, M.F. and Muttoni, A. (2009), "Applications of the critical shear crack theory to punching of RC slabs with transverse reinforcement", *ACI Struct. J.*, **106**(4), 485-494.
- Tovi, S., Goodchild, C. and Ali, B. (2017), "Deformation of multi-storey flat slabs, a site investigation", *Adv. Concrete Constr., Int. J.*, **5**(1), 49-63. <https://doi.org/10.12989/acc.2017.5.1.049>